Journal of Alloys and Compounds, 206 (1994) 55–71
JALCOM 1019

High rare earth sublattice ordering temperatures in RMnSi compounds (R ≡ La–Sm, Gd) studied by susceptibility measurements and neutron diffraction

R. Welter, G. Venturini and B. Malaman*

Laboratoire de Chimie du Solide Minéral, Associé au CNRS UA 158, Université de Nancy I, BP 239, F-54506 Vandoeuvre les Nancy Cedex (France)

(Received September 28, 1993)

Abstract

Investigations by bulk magnetization and neutron diffraction measurements are reported on the ternary silicides RMnSi (R ≡ La–Nd). All these compounds crystallize in the well-known tetragonal structure of the CeFeSi type (space group *P4/nmm*). This structure, which is closely related to the $ThCr_2Si_2$- and $TbFeSi_2$-type structures, can be described as isolated "$ThCr_2Si_2$ blocks" connected via R–R contacts. The R, Mn and Si atoms are arranged in alternate layers stacked along the *c* axis in the sequence R*Si*(Mn_2)*Si*RR*Si*(Mn_2)*Si*R.

All these compounds are antiferromagnetic below $T_N \approx 310$, 240, 265 and 280 K for La-, Ce-, Pr- and NdMnSi respectively. Their magnetic structures are characterized by a stacking of antiferromagnetic (001) Mn layers. The Mn magnetic moments (about 3 μ_B) are at 45° to *c* axis (LaMnSi) or in the (001) plane. At lower temperature PrMnSi and NdMnSi show additional transitions which correspond to an antiferromagnetic ordering of the rare earth sublattice ($T_1 = 130$ and 185 K for Pr and Nd respectively) followed by a spin reorientation process simultaneously with a crystallographic phase transition (tetragonal to orthorhombic symmetry) at about 80 K for both compounds. At 2 K the antiferromagnetic (AF) structure of PrMnSi and NdMnSi consists of a stacking of ferromagnetic and antiferromagnetic (001) layers of R and Mn respectively in the sequence Mn(AF) R(+)R(+) Mn(AF) R(−)R(−); the moments are in the layers, collinear in PrMnSi and in quadrature in NdMnSi. In CeMnSi the ferromagnetic (001) cerium layers order antiferromagnetically below about 175 K and are coupled with the manganese sublattice according to the following scheme: Ce(+) Mn(AF) Ce(+)Ce(−) Mn(AF) Ce(+); at 2 K the Ce moment value is $\mu_{Ce} = 0.78(4)$ μ_B. The results are discussed and compared with those obtained previously for the corresponding ternary silicides and germanides of the CeFeSi-, $TbFeSi_2$- and $ThCr_2Si_2$-type structures.

1. Introduction

Recently we reported on the magnetic properties of RTX (R, rare earth; T ≡ Fe, Ru, Co; X ≡ Si, Ge) compounds [1–4] with the CeFeSi-type structure (*P4/nmm*) [5]. At low temperature these intermetallics present various types of magnetic ordering of the rare earth sublattice, while the transition metal carries no magnetic moment, *i.e.* Fe, Co. The RFeSi [1] compounds were found to be ferromagnetic, while the RCoGe [2], RRuSi(Ge) [3] and RCoSi [4] compounds behave antiferromagnetically. The determination of their magnetic structures allowed us to discern strong similarities between the stacking of the R magnetic sheets in these compounds and that observed in structurally related corresponding compounds with structures of the $ThCr_2Si_2$ [6] and $TbFeSi_2$ [7] type respectively [8].

In another way it is noteworthy that T ≡ Mn is a unique example of a 3d transition metal with a magnetic moment in the $RMnSi_2$ and RMn_2X_2 (X ≡ Si, Ge) compounds [8–10]. The Mn sublattice orders at relatively high temperatures and the structures consist of ferromagnetic Mn sheets coupled ferro- or antiferromagnetically along the stacking axis. From this point of view and in order to complete the comparisons between the magnetic behaviour in these three series, it was very interesting to study the magnetic properties of the corresponding RMnSi *CeFeSi-type* compounds.

The CeFeSi-type silicides RMnSi (R ≡ La–Sm, Gd) were synthesized by Yarovets and Gorenlenko [11] 10 years ago but their magnetic properties were not thoroughly studied. Nikitin *et al.* [12] indicate that LaMnSi and GdMnSi behave ferromagnetically above 295 and 314 K respectively. On the other hand, Kido *et al.* [13] investigated the magnetic and electrical properties of RMnSi (R ≡ Ce, Nd, Sm) compounds above 77 K.

*Author to whom correspondence should be addressed.

SSDI 0925-8388(93)01019-Z

CeMnSi is paramagnetic above 77 K but the authors report that the susceptibility does not follow the Curie–Weiss law below 250 K, indicating antiferromagnetic interactions. In NdMnSi and SmMnSi the Mn sublattice orders antiferromagnetically below $T_N = 153$ and 172 K respectively. There is no magnetic ordering of the R sublattice above 77 K. Furthermore, from interatomic Mn–Mn distance considerations and the occurrence of strongly positive values of the paramagnetic Curie temperatures, these authors concluded the occurrence of ferromagnetic interactions between Mn spins within a layer as observed in the $RMnSi_2$ and RMn_2X_2 compounds. Finally, these authors report a semiconductive behaviour for CeMnSi below about 220 K, whereas NdMnSi and SmMnSi are metallic conductors.

In another way the Mn magnetic ordering of isotypic equiatomic alkali metal manganese pnictides AMnX (A ≡ Li–Cs; X ≡ P–Bi) [14, 15] was deduced from neutron diffraction studies. In this case it is worth noting that the authors found an antiferromagnetic ordering within the dense (001) Mn planes. Therefore it was interesting to check whether this kind of Mn magnetic interaction is typical in the alkali metal pnictides only or may apply also to the equiatomic rare earth manganese silicides.

In this paper we report on the magnetic properties of the RMnSi (R ≡ La–Sm, Gd) compounds by bulk magnetization measurements and neutron diffraction experiments. A comparison with the isotypic $RMnSi_2$ and $RMn_2Si(Ge)_2$ compounds and a more general discussion are given in the conclusion.

2. Crystal structure and structural relationships

The CeFeSi-type structure is a ternary ordered derivative of the Fe_2As type. Its space group is tetragonal *P4/nmm* in which the R (Ce), Fe and Si atoms occupy the 2(*c*) sites $[\frac{1}{4}, \frac{1}{4}, z_R \approx 0.67]$, 2(*a*) sites $[\frac{3}{4}, \frac{1}{4}, 0]$ and 2(*c*) sites $[\frac{1}{4}, \frac{1}{4}, z_{Si} \approx 0.17]$ respectively. The T atoms (*defining a C-centred sublattice*) are embedded in Si tetrahedra connected with each other to build infinite "T_2Si_2" slabs stacking along the *c* axis, whereas the R atoms lie between these slabs in square pyramids of Si atoms (Fig. 1). This structure is closely related to those of $ThCr_2Si_2$ and $TbFeSi_2$. All three structures can be described as being built of alternating square planes containing R, T and Si atoms respectively (Fig. 2). The same "R–Si–T_2–Si–R" block is found in each of them, with the additional R–R sequence in CeFeSi. Figure 2 shows clearly the structural relationships between the three types. Furthermore, according to Parthé and Chabot's classification [16], the "R–Si–T_2–Si–R" slab will be denoted hereafter as the "$BaAl_4$ slab" and

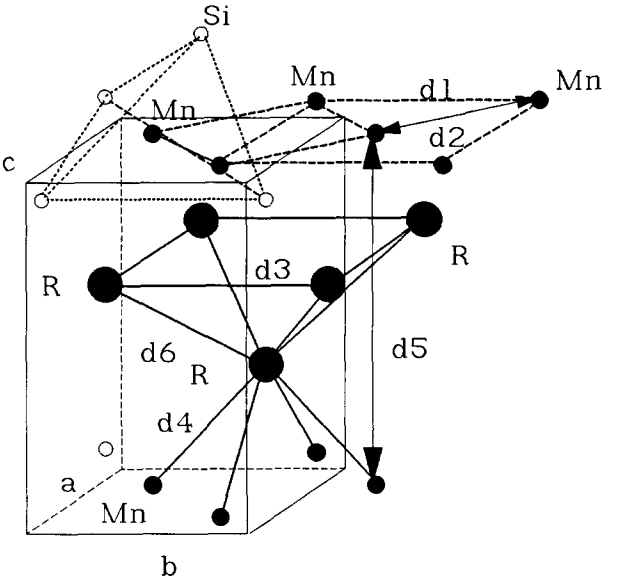

Fig. 1. CeFeSi-type structure of RMnSi compounds.

the R–R slab as the "W slab" (Fig. 2; see also Fig. 1 of ref. 2).

The main interatomic distances between magnetic species calculated in the case of NdMnSi are reported in Table 1, where they can be compared with the corresponding distances in the $ThCr_2Si_2$- and $TbFeSi_2$-type structure compounds.

3. Experimental procedures

The compounds were prepared from commercially available high purity elements. Pellets of stoichiometric mixture were compacted using a steel die and then introduced into silica tubes sealed under argon (100 mmHg). First the samples were heated to 1173 K for preliminary homogenization treatment and then melted in an induction furnace. The resulting ingots were annealed for 2 weeks at 1173 K. The purity of the final product was checked by the powder X-ray diffraction technique (Guinier Cu Kα).

Magnetic measurements were carried out on a Faraday balance (above 300 K) and on a Manics magnetosusceptometer (between 4.2 and 300 K) in fields up to 1.5 T.

Neutron experiments have been carried out at the Institut Laue Langevin (ILL), Grenoble. Several patterns have been collected in the temperature range 1.4–300 K. The diffraction patterns were recorded with the one-dimensional curved multidetector Dlb at a wavelength $\lambda = 2.542$ Å. In order to correct texture effects, following a procedure largely described in ref. 1, we used during the refinements a fitted coefficient (f_{cor}) which reflects the importance of preferential

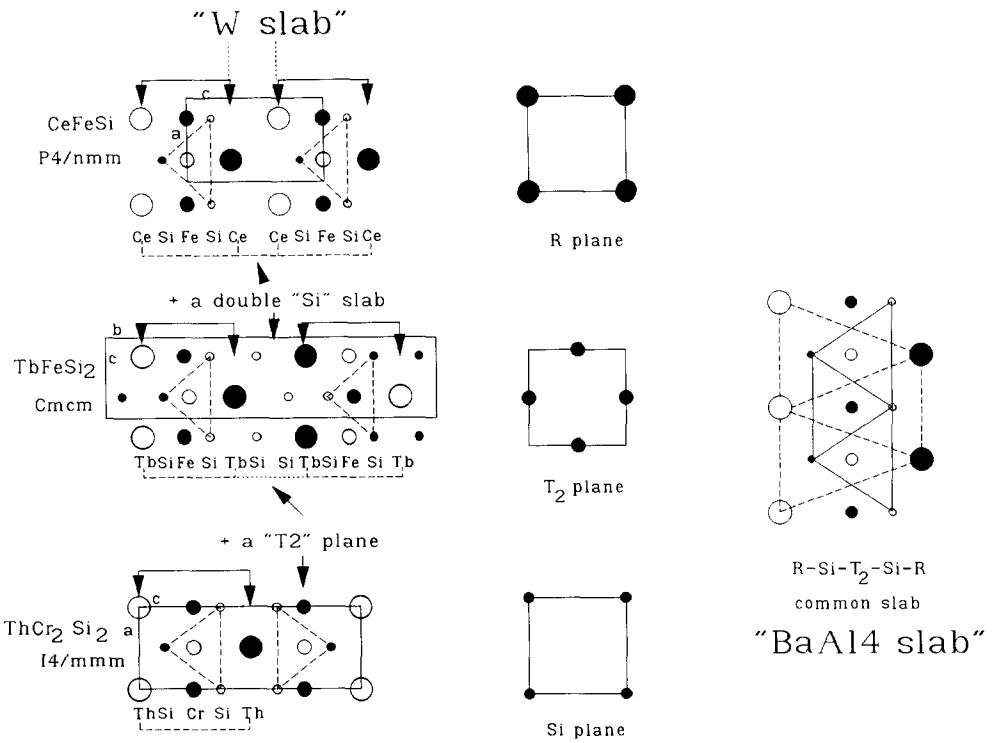

Fig. 2. Structures of CeFeSi, $TbFeSi_2$ and $ThCr_2Si_2$. Structural relationships.

TABLE 1. Main interatomic distances (d) between magnetic species in the CeFeSi-type structure compound NdMnSi (the d_i distances refer to Fig. 1). Comparison with the corresponding distance ranges in $RMn_2Si(Ge)_2$ (d') and $RMnSi_2$ (d'') [8–10]

d_i	Atoms	Type	d (Å)	d' (Å)	d'' (Å)
d_1	Mn–Mn	In plane	4.103	4.19–3.92	4.19–3.99
d_2	Mn–Mn	In plane	2.901	2.97–2.77	2.92–2.84
d_3	Nd–Nd	In plane	4.103	4.19–3.92	4.19–3.99
d_4	Nd–Mn	Interplane	3.210	3.46–3.26	3.30–3.21
d_5	Mn–Mn	Interplane	7.28	5.20–5.49	8.75–8.89
d_6	Nd–Nd	Interplane	3.731 ("CeFeSi typical")		

orientation. The values of f_{cor} obtained (see below) strongly support the validity of this correction.

Using the scattering lengths $b_{Si}=4.149$ fm, $b_{Mn}=-3.73$ fm, $b_{La}=8.29$ fm, $b_{Ce}=4.84$ fm, $b_{Pr}=4.58$ fm and $b_{Nd}=7.69$ fm and the form factors of manganese and rare earth atoms from refs. 17 and 18 respectively, the scaling factor, the z_{Si} and z_R atomic position, f_{cor} and the R and Mn magnetic moments were refined by the mixed crystallographic executive for diffraction (MXD) least-squares-fitting procedure [19].

4. Experimental results

Our syntheses confirm that the RMnSi *CeFeSi-type structure* series extends from LaMnSi to GdMnSi at 1173 K. Lattice parameters refined at room temperature (see Tables 3–6) are in quite good agreement with the earlier published values [11–13]. Their evolution with the radius of the rare earth atom suggests that cerium is probably in a trivalent state in CeMnSi. This is confirmed by L_{III} absorption experiments [20].

4.1. Susceptibility measurements

The main characteristic magnetic data are collected in Table 2 and displayed in Figs. 3(a) and 3(b).

Within the studied compounds (R ≡ La–Sm, Gd) only GdMnSi exhibits a spontaneous magnetization over the whole ordering temperature range. The magnetic curve is characterized by a Curie point at 310 K and an inflection point at 300 K, in agreement with Nikitin *et al.* [12], who nevertheless do not detect the second transition. These two magnetic transition temperatures are probably related to the ordering of the Mn and Gd sublattices respectively (Fig. 3(a)). At 4.2 K the maximum magnetization moment value (4.9 μ_B) rather indicates a ferrimagnetic arrangement of the two ferromagnetic sublattices. The hysteresis loop does not indicate any coercive effects.

The lanthanum and cerium samples behave as paramagnetic compounds in the whole temperature range (Fig. 3(b)). This is in contradiction with the results of Nikitin *et al.* [12], who assume a ferromagnetic ordering of LaMnSi. According to their values of the Curie temperature (295 K) and the maximum magnetization

TABLE 2. RMnSi: magnetic data

Compound	Bulk magnetization measurements					Neutron diffraction data				
	$T_{C,N}$ ±2 (K)	θ_P (K)	μ_{eff} (μ_B)	$\mu_{eff,Mn}$ (μ_B)	μ_{max} (μ_B) (4.2 K, 15 kOe)	T_N ±10 (K)	T_1 ±5 (K)	T_2 (K)	μ_{Mn} (μ_B) (2 K)	μ_R (μ_B) (2 K)
LaMnSi		−350	3.07	3.07		310			3.27	
CeMnSi		−50	3.80	2.83		240	175		2.97	0.80
PrMnSi	130, 80	75	4.69	3.03		265	130	80(10)	2.96	2.54
NdMnSi	175, 80	110	4.60	2.84		280	185	80(10)	2.80	2.54
SmMnSi	235, 220, 110									
GdMnSi	310, 300	265	8.52	3.10	4.89					

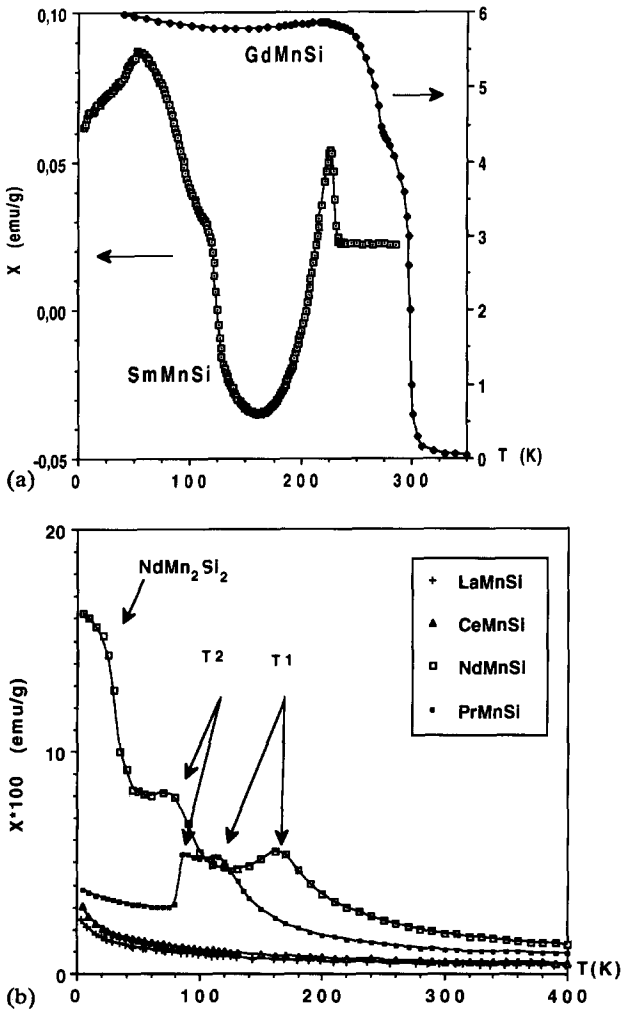

Fig. 3. (a) Temperature dependence of the susceptibility in GdMnSi and SmMnSi measured at $H=100$ G; (b) temperature dependence of susceptibility in LaMnSi, CeMnSi, PrMnSi and NdMnSi measured at $H=10$ kG.

moment measured at 4.2 K (0.24 μ_B), their results rather seem to indicate very small amounts of $LaMn_2Si_2$ [8] in their sample. On the contrary, our results are in good accordance with those of Kido *et al.* [13], who found a paramagnetic behaviour for CeMnSi down to 77 K.

The other paramagnetic rare earth compounds (R ≡ Pr–Sm) exhibit globally antiferromagnetic behaviours with, in each case, several transitions below room temperature (Table 2 and Figs. 3(a) and 3(b)). It is worthwhile to note the complex low field behaviour of the samarium compound.

Except for SmMnSi, the temperature dependence of the inverse susceptibilities above room temperature obeys a Curie–Weiss-type law with large negative paramagnetic Curie temperatures θ_P for the lanthanum and cerium compounds.

Finally it should be noted that in the antiferromagnetic PrMnSi and NdMnSi compounds θ_P is positive, in contrast with normal behaviour, as already noted by Kido *et al.*

In order to specify the magnetic behaviour of these compounds, we have undertaken neutron diffraction experiments. SmMnSi and GdMnSi have not been studied, since the samarium and gadolinium absorption coefficients are too large at the wavelength used (2.542 Å).

Remark: Additional DTA measurements were undertaken after the neutron study. They do not allow us to detect any anomaly around the Néel temperature deduced from the neutron diffraction results.

4.2. Neutron diffraction study

4.2.1. Crystal structure

At 300 K the neutron diffraction patterns of CeMnSi, PrMnSi and NdMnSi are characteristic of only nuclear scattering (see below). The extinction rules of the space group *P4/nmm* are fulfilled and confirm unambiguously the CeFeSi-type structure for these compounds. Attempts to fit the nuclear lines by interchanging the positions of the manganese and silicon atoms lead to poorer agreement and give no evidence for any mixing between the manganese and silicon atoms at 2(*a*) and 2(*c*) sites. A comparison between the observed and

calculated intensities of the nuclear peaks for each compound is given together with the z_R and z_{Si} values, f_{cor}, the reliability factors and the lattice parameters in the tables of the corresponding sections.

4.2.2. LaMnSi

Several patterns were recorded in the temperature range 300–1.4 K (Fig. 4).

All the patterns exhibit an additional line which can be indexed on the basis of the crystal unit cell as (100) (*forbidden by the nuclear space group P4/nmm*). This result is characteristic of an antiferromagnetic ordering not detected in the bulk susceptibility measurements (see Section 4.1). Furthermore, magnetic contributions occur under nuclear (*hkl*) lines with $h+k=2n+1$ as indicated by the increase in their intensities together with those of the (100) line when the temperature decreases (Fig. 4). These observations indicate an anti-C ordering, giving evidence of an antiferromagnetic arrangement of the Mn moments within the (001) plane. Such magnetic structure is identical with that determined by Bronger *et al.* [14] and Muller *et al.* [15] in the alkali metal manganese pnictides. The best refinements lead to Mn moment values of 1.92(9) and 3.27(4) μ_B at 280 and 1.4 K respectively. Over the whole temperature range their direction makes an angle of 45(1)° with the *c* axis. The magnetic structure is drawn in Fig. 5. It consists of a stacking of antiferromagnetic (001) Mn layers, the manganese moments being ferromagnetically coupled with their direct neighbours situated in each adjacent plane along the *c* axis. The thermal variation in the Mn moment gives a Néel temperature $T_N \approx 310(10)$ K (Fig. 6). Table 3 gives the observed and calculated intensities together with the lattice constants and the various adjustable parameters at 280 and 1.4 K.

4.2.3. CeMnSi

Several patterns were recorded in the temperature range 300–1.4 K.

Below about 250 K the characteristics of the neutron diffraction patterns are similar to those observed for LaMnSi, yielding the same antiferromagnetic ordering on the Mn sublattice. Nevertheless, in this case the best refinements show that the Mn moments are in the (001) plane. Furthermore, below about 200 K some discrepancies remain within the magnetic intensities.

Since the particular indexing (see Section 4.2.2) of the lines with magnetic contributions does not allow us to invoke any other arrangement of the manganese moments (antiferromagnetic (001) plane), magnetic ordering of the Ce sublattice has to be considered in agreement with the trivalent state of Ce atoms in this compound (Section 4.1). The results of the refinements carried out in this direction are collected in Table 4. They display the presence of a weak moment on cerium which becomes significant below 200 K and increases to 0.8 μ_B at 1.4 K. The resulting magnetic structure is shown in Fig. 7. It consists of an alternating stacking of antiferromagnetic Mn layers and two ferromagnetic Ce layers of opposite magnetization. The moments of both the Mn and Ce sublattices are in the (001) plane and collinear, each sublattice being antiferromagnetic. Apart from the orientation of the moments, the magnetic arrangement of the Mn sublattice is the same as in LaMnSi but with slightly smaller moment values (1.5

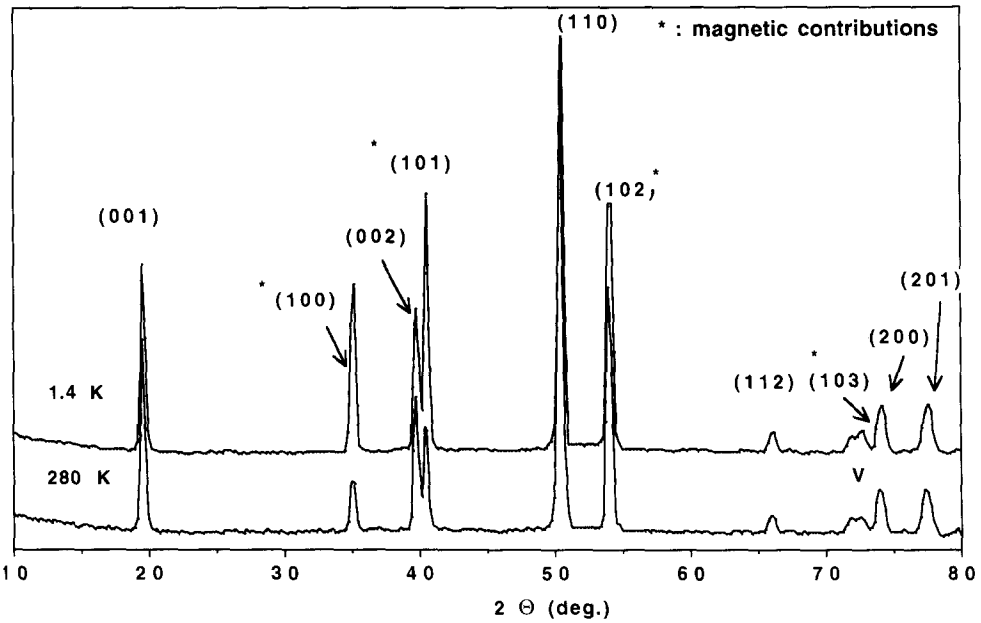

Fig. 4. Neutron diffraction patterns of LaMnSi at 280 and 1.4 K.

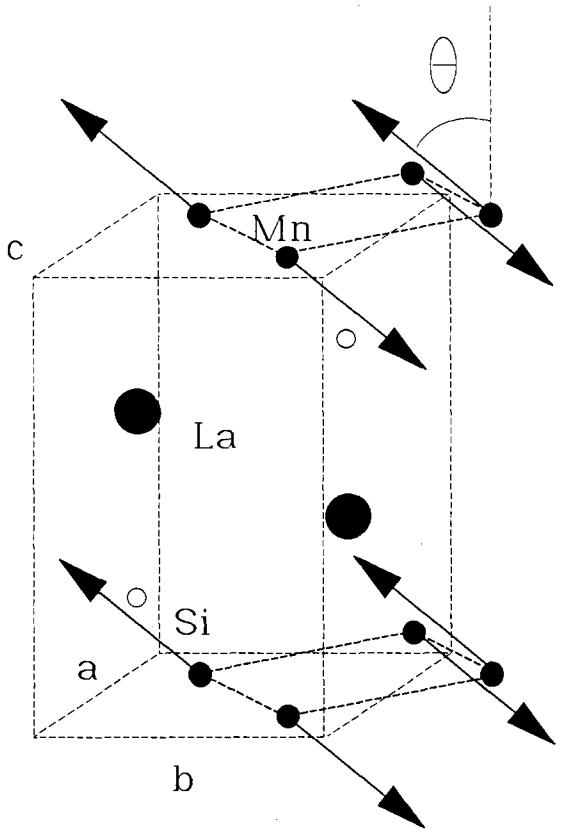

Fig. 5. Magnetic structure of LaMnSi.

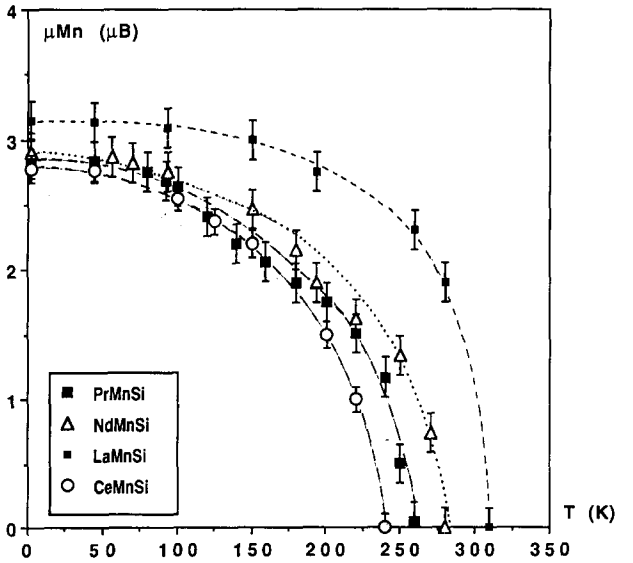

Fig. 6. Temperature dependence of manganese magnetic moment in LaMnSi, CeMnSi, PrMnSi and NdMnSi.

and 2.7 μ_B at 180 and 1.4 K respectively). The Ce–Ce couplings are antiferromagnetic within the "W slab" and the "$BaAl_4$ slab", giving rise to the + − + − sequence. Since the Ce–Mn distances are all chemically equivalent, the magnetic couplings between the two species may be defined as follows: (i) one assumes that

TABLE 3. LaMnSi: observed and calculated intensities and refined parameters at 280 and 1.4 K

h k l	280 K		1.4 K	
	I_o	I_c	I_o	I_c
0 0 1	290(1)	288	290(1)	291
1 0 0	240(1)	248	781(3)	777
0 0 2	786(3)	772	833(4)	823
1 0 1	695(4)	683	1500(11)	1530
1 1 0	4346(12)	4318	4530(15)	4510
1 0 2	2683(9)	2720	3072(8)	3168
1 1 2	320(6)	412	413(8)	524
2 0 0	1231(11)	1245	1304(16)	1300
2 0 1	1384(15)	1493	1336(14)	1327
a (Å)	4.181(3)		4.185(1)	
b (Å)	7.388(5)		7.417(3)	
z_{Si}	0.207(3)		0.208(2)	
z_{La}	0.664(2)		0.668(1)	
r_{cor}	1.07(1)		1.07(1)	
μ_{Mn} (μ_B)	1.92(9)		3.27(4)	
θ (°)	45(1)		45(1)	
R (%)	2.5		3.5	

the Ce moment lies along the [010] direction; (ii) one defines the (P) plane perpendicular to this direction and containing the Ce atom; (iii) the two Mn nearest neighbours which belong to this plane are ferromagnetically coupled with the Ce moment, while the two Mn neighbours outside the (P) plane are antiferromagnetically coupled with the cerium atom.

The thermal variations in the magnetic moments give Néel temperatures T_N of 240 and 175 K for the Mn and Ce sublattices respectively (Figs. 6 and 8). It is noteworthy that such magnetic transitions are not detected by bulk magnetic measurements and differential thermal analysis (see Section 4.1) or by electrical resistivity experiments [13]. Nevertheless, it is noteworthy that the first transition corresponds to the anomaly in the behaviour of the susceptibility observed by Kido *et al.* [13]. Moreover, the shape of the L_{III} absorption edge is unchanged between 10 and 300 K. This clearly indicates that the valence of the cerium ion does not change in the whole temperature range [14].

Table 4 gives the observed and calculated intensities together with the lattice constants and the various adjustable parameters.

4.2.4. PrMnSi

The temperature dependence of the neutron diffraction patterns recorded step by step from room temperature to 2 K shows the following.

(1) below 265 K additional lines appear in the neutron diffraction patterns (Fig. 9), while the remaining lines are characteristic of only nuclear scattering with no magnetic contributions. The additional lines are char-

TABLE 4. CeMnSi: observed and calculated intensities and refined parameters at 300, 180, 102 and 1.4 K. I_{c1} refers to hypothesis (1) with zero net moment on the cerium site; I_{c2} refers to hypothesis (2) with a moment on the cerium atoms (see Section 4.2.3)

$h\ k\ l$	300 K		180 K			102 K			1.4 K		
	I_o	I_c	I_o	I_{c1}	I_{c2}	I_o	I_{c1}	I_{c2}	I_o	I_{c1}	I_{c2}
0 0 1	75	75	73	72	72	74	73	73	79	77	77
1 0 0	0	0	45	54	44	102	140	101	92	161	90
0 0 2	271	273	275	277	279	278	287	279	280	299	279
1 0 1	0	1	126	114	127	353	290	349	477	346	469
1 1 0	1438	1431	1428	1425	1427	1435	1405	1428	1465	1389	1458
1 0 2	634	636	731	731	730	872	888	884	978	982	970
1 1 1	118	109	129	119	120	146	120	124	146	121	150
0 0 3	24	16	24	17	16	17	18	16	21	20	16
1 1 2	58	55	92	61	63	57	57	73	79	91	91
1 0 3	110	88	143	129	130	258	232	238	284	272	278
2 0 0	212	239	226	238	238	230	234	238	221	231	243
2 0 1	384	402	361	381	383	343	375	388	418	369	402
			(1)		(2)	(1)		(2)	(1)		(2)
a (Å)	4.125(1)			4.120(1)			4.114(1)			4.117(2)	
c (Å)	7.285(2)			7.306(3)			7.300(3)			7.293(3)	
z_{Si}	0.200(1)		0.198(2)		0.198(1)	0.197(7)		0.199(2)	0.195(9)		0.198(1)
z_{Ce}	0.665(1)		0.668(2)		0.668(2)	0.668(4)		0.668(1)	0.665(9)		0.669(1)
r_{cor}	1.09(1)		1.08(1)		1.08(1)	1.07(2)		1.09(1)	1.05(4)		1.10(1)
μ_{Mn} (μ_B)	0		1.48(5)		1.50(4)	2.36(10)		2.45(3)	2.56(15)		2.72(3)
μ_{Ce} (μ_B)	0		0		0.16(7)	0		0.41(5)	0		0.78(4)
R (%)	2.1		2.7		2.5	5.1		3.2	9.4		1.9

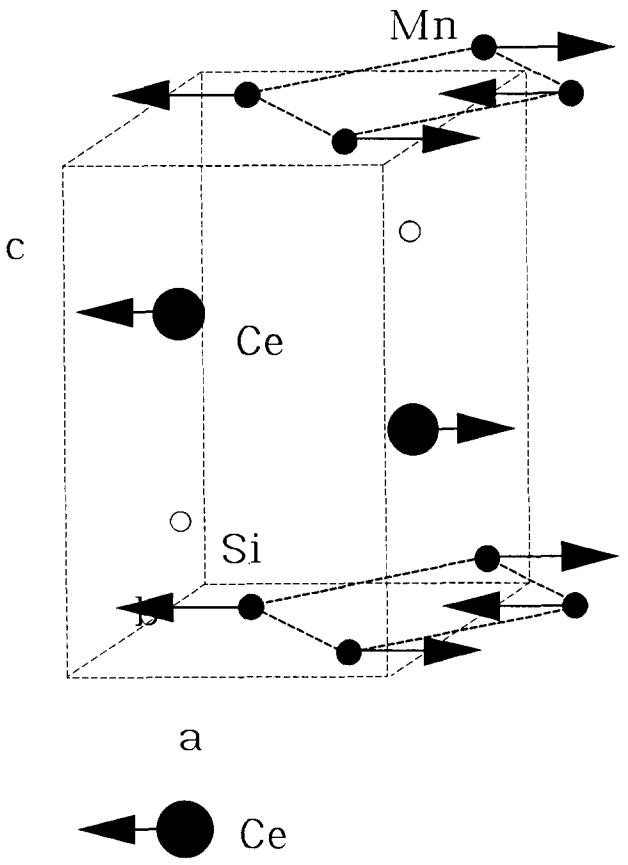

Fig. 7. Magnetic structure of CeMnSi at 1.4 K.

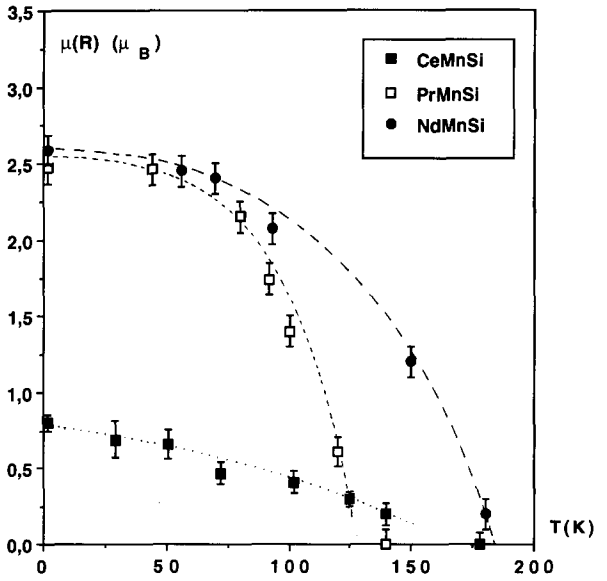

Fig. 8. Temperature dependence of rare earth magnetic moment in CeMnSi, PrMnSi and NdMnSi.

acteristic of an antiferromagnetic ordering below $T_N \approx 265$ K, in contrast with the magnetic measurements. The Bragg angles of these superlattice lines can all be indexed on the basis of a magnetic unit cell (m) twice large as the chemical one (c) by doubling the c axis (*i.e.* a wavevector $\boldsymbol{k}=(0, 0, \frac{1}{2})$) and obey the rule (*hkl*/2) with $h+k=2n+1$.

(2) Below $T_1=130$ K two additional lines indexed as $(00\frac{1}{2})$ and $(11\frac{1}{2})$ appear and increase slowly (Fig. 9).

(3) Below $T_2=80$ K the intensity of the various magnetic lines changes and a splitting (clearly observed at 2 K in Fig. 10) of all the (*h0l*) lines (nuclear and magnetic) occurs.

All these observations imply an antiferromagnetic ordering for both the Mn and Pr sublattices below 265 and 130 K respectively. In addition, at low temperature a strong magnetostriction effect occurs, yielding a crystallographic phase transition at $T_2=80$ K. It is noteworthy that T_1 and T_2 have been detected by bulk magnetization measurements (see Section 4.1). Finally, the variation in the intensities of the $(00\frac{1}{2})$ and $(10\frac{3}{2})$ magnetic lines (Fig. 11) clearly indicates the occurrence of three different magnetic states on decreasing the temperature from 300 to 2 K.

Four neutron diffraction patterns recorded at 275, 200, 91 and 2 K are shown in Fig. 9.

4.2.4.1. $T_N=260>T>T_1=130$ K. The occurrence of the magnetic lines (*hkl*/2) with $h+k=2n+1$ implies an anti-C ordering mode as already observed in LaMnSi. In addition, owing to the doubling of the c axis, the moments have to be inverted on each successive (001) antiferromagnetic Mn plane. The best refinement corresponds to the Mn moments lying in the basal (001) plane (Fig. 12(a)) with a refined value $\mu_{Mn}=1.82(3)$ μ_B at 180 K. Its thermal evolution (Fig. 6) gives a Néel temperature of 265(5) K. It is noteworthy that, in contrast with the La and Ce compounds, the interlayer coupling between nearest Mn atoms is this time antiferromagnetic, yielding the doubling of the cell along the c axis.

4.2.4.2. $T_1=130>T>T_2=80$ K. This temperature range is characterized by the growth of the two magnetic peaks $(00\frac{1}{2})$ and $(11\frac{1}{2})$, yielding the disappearance of the anti-C ordering mode (Fig. 9), and the $(00\frac{3}{2})$ peak is absent.

For an Mn sublattice rearrangement only, the structure factor of the (003) (*in the magnetic cell*) line is given by

$$F(003)_{Mn} \propto M'_1+M'_2-M'_3-M'_4$$

where M'_1 and M'_2 are the Mn moments lying in $z=0$, M'_3 and M'_4 in $z=\frac{1}{2}$ and $M'_1=M'_2$, $M'_3=M'_4$ (*C mode*) and $M'_1=-M'_3$ (*antiferromagnetic arrangement*), yielding $F(003)_{Mn}=0$. Thus the occurrence of these new lines corresponds only to an antiferromagnetic ordering of the Pr sublattice taking place at $T_1=130$ K.

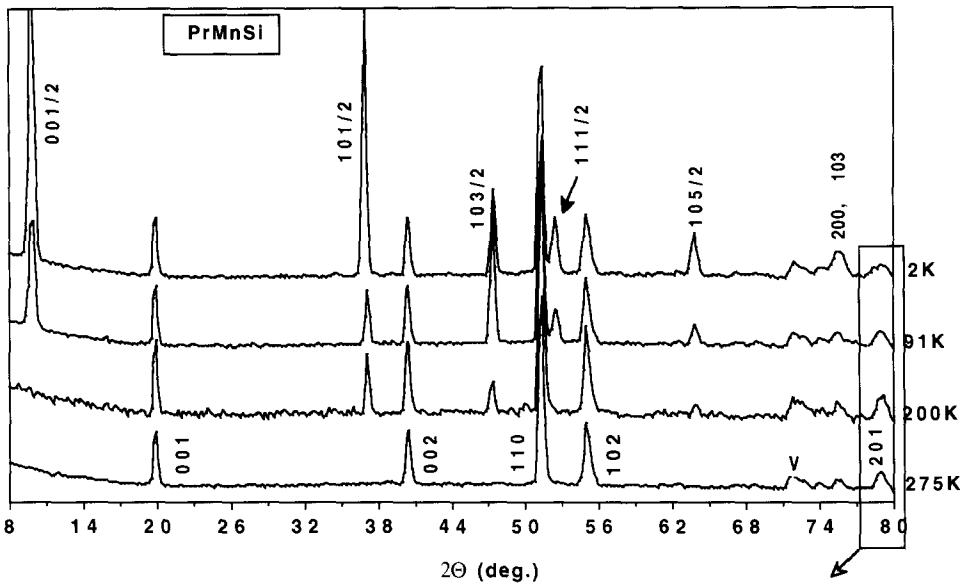

Fig. 9. Neutron diffraction patterns of PrMnSi at 275, 200, 91 and 2 K.

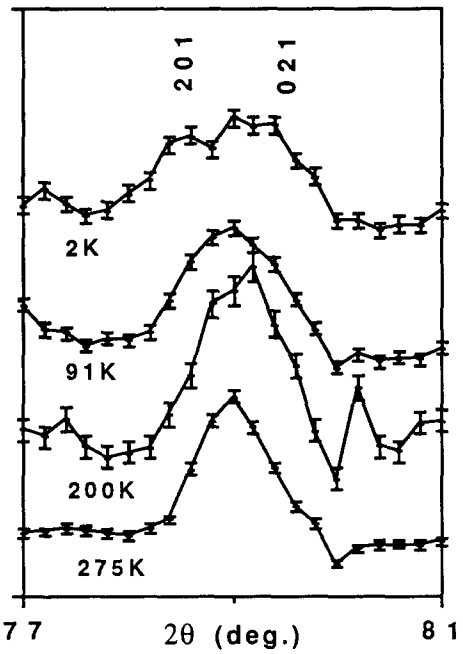

Fig. 10. Detailed view of neutron diffraction patterns of PrMnSi (see Fig. 9) showing occurrence of a splitting of the (201) line below about 80 K (see text).

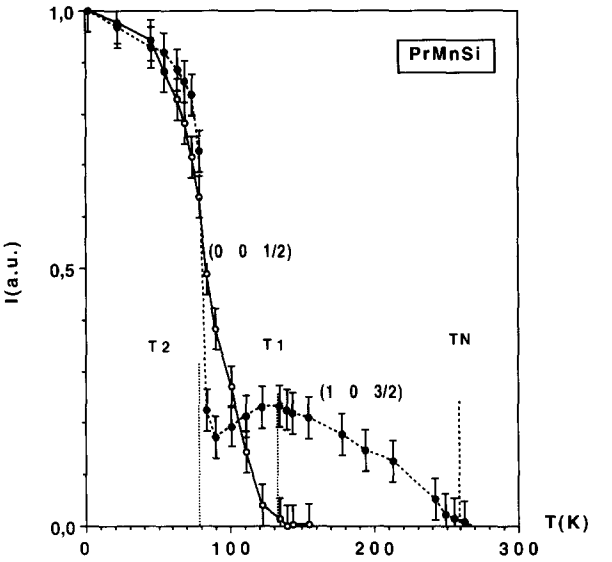

Fig. 11. PrMnSi: temperature dependence of integrated intensities of $(10\frac{3}{2})$ and $(00\frac{1}{2})$ lines.

Furthermore, under these conditions the zero net value of the $(00\frac{3}{2})$ line implies that the magnetic arrangement of the Pr sublattice consists of ferromagnetic (001) planes with a $++--$ coupling sequence along the c axis. In fact, the structure factor of the (003) (*in the magnetic cell*) line is now given by (the Mn contribution being zero; see above)

$$F(003)_{Pr} \alpha -M_1+M_2+M_3-M_4$$

where M_i are the successive Pr moments along the c axis in the magnetic cell, *i.e.* $z \approx \frac{1}{6}, \frac{1}{3}, \frac{2}{3}$ and $\frac{5}{6}$ (Fig. 12(b)), and $M_1=M_2$, $M_3=M_4$ and $M_1=-M_3$ ($++--$ sequence), yielding $F(003)=0$.

The best refinement gives a collinear antiferromagnetic structure with the Mn and Pr moments lying in the (001) plane (Fig. 12(b)). At 91 K the moment values are 2.69(3) and 1.64(1) μ_B for Mn and Pr respectively. The ferromagnetic (001) Pr layers are ferromagnetically coupled within the "W slab" and antiferromagnetically coupled within the "$BaAl_4$ slab". Assuming the same definition of the (P) plane as in CeMnSi, the moments of the Mn atoms lying in (P)

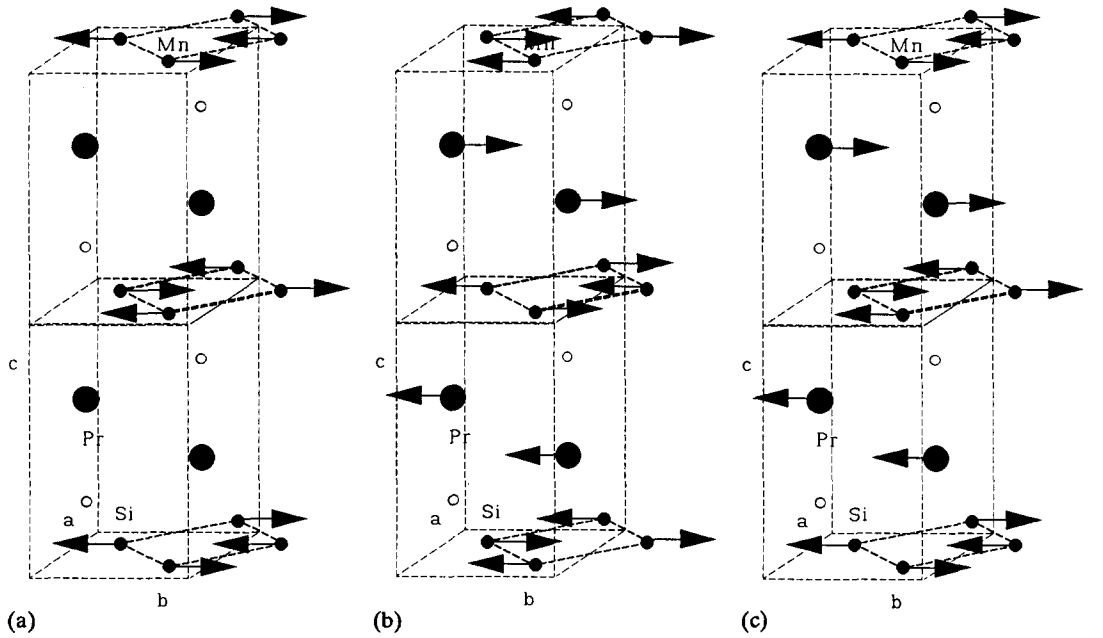

Fig. 12. Magnetic structure of PrMnSi at (a) 300, (b) 100 and (c) 2K.

are ferromagnetically coupled to the Pr ones, while those which are outside (P) are antiferromagnetically coupled to the Pr moments.

4.2.4.3. $T<T_2=80$ K. Below 80 K new changes in the magnetic intensities occur and the (*h0l*) lines split significantly into two components (Fig. 10). Therefore a strong magnetostriction effect connected with a spin reorientation of the Mn or Pr (or both) sublattice occurs at $T_2=80$ K, yielding a crystallographic phase transition from tetragonal to orthorhombic symmetry. Owing to the absence of the (100) and (010) nuclear lines, the new space group becomes *Pmmn*. The thermal variation in the a_o and b_o lattice parameters is shown in Fig. 13, assuming $a_o>b_o$.

The best fits show unambiguously that the change in the magnetic intensities involves a spin reorientation (a 180° rotation) of the Mn sublattice alone. The magnetic structure is shown in Fig. 12(c). Here again it is collinear with the same couplings within each magnetic sublattice. Therefore the magnetic structure modification concerns only the magnetic interactions between the Pr and Mn sublattices. According to the orthorhombic symmetry, the fits also show clearly that the moments are aligned along the b_o axis, *i.e.* along the smallest lattice constant. Since the structural distortion splits the four shortest Pr–Mn distances into two sets of distances, the new magnetic structure may be described as follows: the Pr and Mn moments corresponding to the shortest contact (in the (b_oc_o) plane, *i.e.* the (P) plane defined previously) are now ferromagnetically coupled, while the Pr–Mn interactions

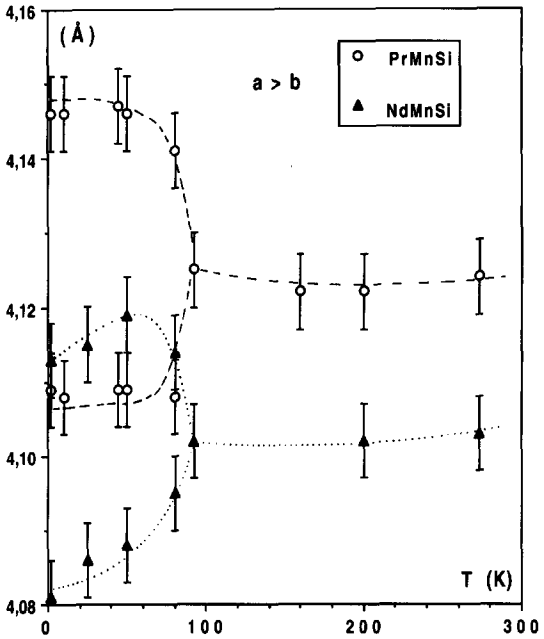

Fig. 13. Temperature dependence of lattice parameters in PrMnSi and NdMnSi.

corresponding to the next-nearest distances ((a_oc_o) plane) are antiferromagnetic.

At 2 K the Mn magnetic moment is found to be $\mu_{Mn}=2.86(2)\ \mu_B$, a value which is in fair agreement with those observed in LaMnSi and CeMnSi. For the Pr atom a moment value $\mu_{Pr}=2.42(1)\ \mu_B$ ($gJ=3.20\ \mu_B$) is obtained, indicating that the praseodymium magnetic moment is slightly quenched by the crystalline electric field (EFG) effect. Its thermal evolution (Fig. 8) gives

a Néel temperature T_1 of 130(5) K. The spin reorientation temperature deduced from the thermal evolution of the intensities of the $(00\frac{1}{2})$ and $(10\frac{3}{2})$ magnetic lines (Fig. 11) is $T_2=80(5)$ K. These results are in good agreement with the bulk magnetic measurements.

Table 5 gives the observed and calculated intensities together with the lattice constants and the various adjustable parameters at 275, 200, 91 and 2 K.

4.2.5. NdMnSi

Neutron diffraction patterns recorded step by step between 300 and 1.4 K reveal the same magnetic and crystallographic behaviours. According to the variation in the $(00\frac{1}{2})$ and $(10\frac{1}{2})$ lines (Fig. 14), the transition temperatures are $T_N=280$ K, $T_1=185$ K and $T_2=80$ K.

Between room temperature and 80 K the patterns are very similar to those observed for PrMnSi, yielding the same magnetic ordering of the Mn and Nd sublattices (Figs. 12(a) and 12(b)). At 93 K $\mu_{Mn}=2.75(4)$ μ_B and $\mu_{Nd}=2.07(3)$ μ_B. These values are close to those observed in PrMnSi.

Below 80 K the change in the magnetic intensities and the splitting of the $(h0l)$ lines originate from the same strong magnetostriction effect connected with a similar crystallographic phase transition (Fig. 13) and spin reorientation of the Mn sublattice as in PrMnSi. Here again it is noteworthy that T_1 and T_2 have been detected by magnetic measurements (see Section 4.1).

The magnetic structure at 2 K is shown in Fig. 15. Here again the same couplings within each magnetic sublattice occur. Nevertheless, this time the best fits lead to a spin reorientation of the Mn sublattice of only about 90°. Therefore the moments are in the (001) plane and are aligned along the b_o and a_o axis for Nd and Mn respectively (assuming $a_o>b_o$).

The thermal variations in the magnetic moments of Mn and Nd are shown in Figs. 6 and 8. At 2 K the Mn magnetic moment is found to be $\mu_{Mn}=2.97(3)$ μ_B, a value which is in fair agreement with those observed in previous RMnSi compounds. For the Nd atom a moment value $\mu_{Nd}=2.59(1)$ μ_B ($gJ=3.28$ μ_B) is obtained, indicating that the neodymium magnetic moment (like the Pr one) is slightly quenched by the EFG effect.

Table 6 gives the observed and calculated intensities together with the lattice constants and the various adjustable parameters at 300, 194, 93 and 2 K.

TABLE 5. PrMnSi: observed and calculated intensities and refined parameters at 275, 200, 91 and 2 K

$h\ k\ l$	275 K		200 K		91 K		2 K	
	I_o	I_c	I_o	I_c	I_o	I_c	I_o	I_c
0 0 $\frac{1}{2}$					121(1)	121	325(1)	323
0 0 1	223(1)	227	221(1)	221	225(1)	227	223(1)	220
1 0 $\frac{1}{2}$			556(2)	560	606(3)	614	3008(5)	2993
0 0 2	886(3)	858	878(3)	870	861(4)	844	874(3)	871
1 0 1					26(3)	29		
1 0 $\frac{3}{2}$			581(3)	541	2331(9)	2309	1614(6)	1681
1 1 0	4668(5)	4646	4744(7)	4725	4689(7)	4533	4832(9)	4895
1 1 $\frac{1}{2}$					403(9)	386	876(7)	943
1 0 2	1713(4)	1724	1817(4)	1817	1575(6)	1567	2297(8)	2264
1 1 1	337(5)	391	385(7)	370	295(9)	339	340(6)	312
1 0 $\frac{5}{2}$			527(7)	400	764(8)	789	1562(8)	1592
1 0 3								
2 0 0	678(8)	718	650(9)	702				
1 1 $\frac{5}{2}$					1037(9)	970		
2 0 $\frac{1}{2}$					292(7)	308	2641(9)	2646
2 0 1	1326(9)	1358	1351(9)	1321	1479(8)	1345	1368(7)	1350
a (Å	4.124(1)		4.124(1)		4.124(1)		4.141(3)	
b (Å)	4.124(1)		4.124(1)		4.124(1)		4.107(3)	
c (Å)	7.307(5)		7.307(5)		7.307(5)		7.298(7)	
z_{Si}	0.205(3)		0.202(2)		0.209(3)		0.200(1)	
z_{Pr}	0.664(2)		0.666(1)		0.665(2)		0.666(1)	
r_{cor}	1.11(1)		1.11(1)		1.10(1)		1.106(3)	
μ_{Mn} (μ_B)			1.83(4)		2.69(3)		2.86(2)	
μ_{Pr} (μ_B)					1.64(1)		2.42(1)	
R (%)	3.5		2.7		3.5		3.5	

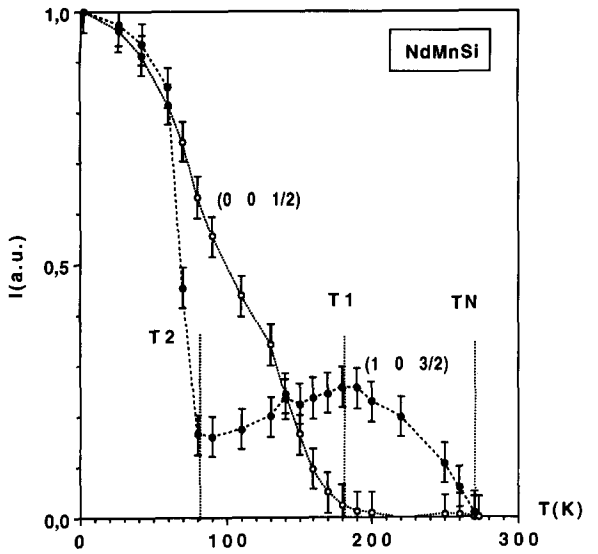

Fig. 14. NdMnSi: temperature dependence of integrated intensities of $(10\frac{3}{2})$ and $(00\frac{1}{2})$ lines.

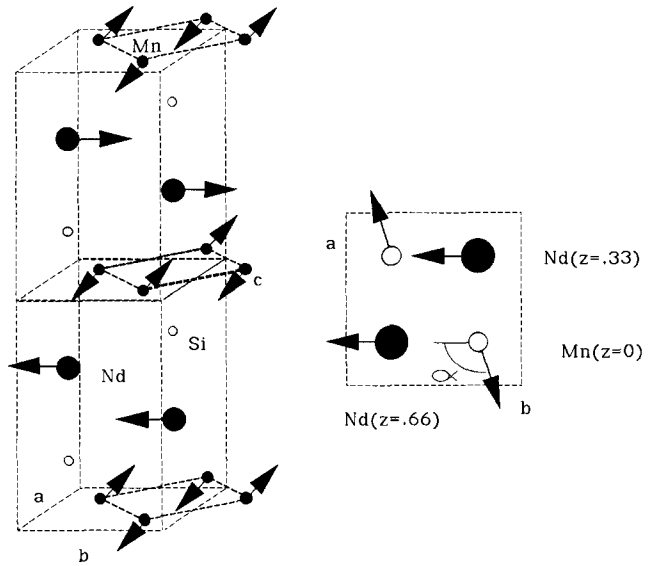

Fig. 15. Magnetic structure of NdMnSi at 2 K.

The various transition temperatures deduced from this neutron study are collected in Table 2.

5. Discussion

The neutron diffraction study implies strong revisions of previous magnetic data reported for the RMnSi series [12, 13]. One of the main results is the occurrence of an antiferromagnetic ordering on the Mn sublattice near room temperature not detected by magnetization measurements. Moreover, in the case of Pr and Nd the transition temperatures deduced from the thermal susceptibility behaviour are due to an antiferromagnetic ordering of the R sublattice followed by a spin reorientation process within the Mn sublattice.

The magnetic behaviour of rare earth (R) –transition metal (T) systems where T is a magnetic 3d element is a complex problem which is up to now not well understood. Thus the discussion will be only phenomenological and limited to some comparisons with the magnetic behaviour of the known compounds isotypic with CeFeSi-, $TbFeSi_2$- and $ThCr_2Si_2$-type structures.

In Section 1 we have emphasized the direct relationships between these three structures. The CeFeSi-type structure can be described as isolated $ThCr_2Si_2$-type blocks (containing the Mn (001) planes) connected via R–R contacts; these "$BaAl_4$" blocks are connected by Si–Si slabs in $TbFeSi_2$. Here, as in the corresponding RMn_2X_2 (X≡Si, Ge) and $RMnSi_2$ compounds, we observed magnetic ordering of the Mn sublattice. The magnetic properties of the two latter series have been widely described and discussed [9, 10] (*see also ref.* 8, *where an extensive review on the magnetic properties of* RMn_2X_2 *can be found*). We will just recall hereafter the main conclusions.

In the pseudolamellar structures of these different ternary compounds there are the same Mn atom planes with a tetrahedral coordination of the non-metal atoms: (010) planes in $TbFeSi_2$ and (001) in the isotypic $ThCr_2Si_2$ compounds. The distances between Mn atoms are short: $2.97 > d_{Mn-Mn} > 2.74$ Å (Fig. 1). In these planes the magnetic interactions remain nearly of the same magnitude in the two series. They are always ferromagnetic (easy axis) and probably strong, in agreement with the Slater–Néel curve and the experimental Curie temperatures [8–10]. The interlayer interactions should be weaker than those acting within the planes. Superexchange couplings via Si or Ge atoms have been proposed but not really confirmed. Nevertheless, it was shown that the sign of the Mn–Mn interlayer exchange coupling appears to be a sensitive function of the lattice parameters, *i.e.* the Mn–Mn separation. The critical Mn–Mn distance for the transition from antiferromagnetism to ferromagnetism is $d_2 \approx 2.85$ Å within the layer and $d_5 \approx 5.29$ Å between layers (Table 1).

In this respect the magnetic properties of the RMnSi compounds are surprising, since the Mn layers ($d_2 \approx 2.9$ Å) order antiferromagnetically with an easy plane anisotropy direction. Furthermore, the interlayer interactions between nearest neighbours in adjacent planes are ferromagnetic in LaMnSi and CeMnSi but antiferromagnetic in PrMnSi and NdMnSi ($d_5 \approx 7.3$ Å, Table 1). In addition, bulk susceptibility measurements and differential thermal analysis do not evidence the ordering point of the manganese sublattice in the RMnSi compounds. Such results are in good accordance with the study of Kido *et al.* [13], who did not report any room temperature ordering of the Mn moments either by magnetization or by electrical resistivity measurements.

TABLE 6. NdMnSi: observed and calculated intensities and refined parameters at 300, 194, 93 and 2 K

$h\ k\ l$	300 K		194 K		93 K		2 K	
	I_o	I_c	I_o	I_c	I_o	I_c	I_o	I_c
0 0 $\frac{1}{2}$					32.6(1)	35	60(1)	59
0 0 1	70(1)	70	70(1)	69	70(1)	70	70(1)	71
1 0 $\frac{1}{2}$			93(1)	94	77(1)	85	334(2)	334
0 0 2	202(2)	202	198(2)		205(3)	191	185(3)	183
1 0 1	72(1)	67	68(1)	61	60(2)	58	61(2)	58
1 0 $\frac{3}{2}$			94(2)	90	472(5)	464	387(5)	387
1 1 0	1156(5)	1158	1104(4)	1104	1114(9)	1115	1130(9)	1126
1 1 $\frac{1}{2}$					104(3)	96	139(5)	149
1 0 2								
1 1 1	610(4)	607	565(3)	570	604(6)	622	598(5)	608
1 0 $\frac{5}{2}$			54(5)	60	147(5)	145	250(6)	254
1 1 2	118(5)	107	90(4)	101	90(6)	104	76(7)	79
1 0 3	102(6)	112	123(9)	115	104(7)	120	156(8)	132
2 0 0	314(8)	311	304(5)	296				
1 1 $\frac{5}{2}$					370(8)	403		
2 0 $\frac{1}{2}$					82(7)	80	618(8)	605
2 0 1	365(9)	379	364(8)	370	391(9)	388	350(9)	355
a (Å)	4.103(2)		4.102(1)		4.102(3)		4.113(2)	
b (Å)	4.103(2)		4.102(1)		4.102(3)		4.081(2)	
c (Å)	7.284(5)		7.288(5)		7.288(7)		7.285(5)	
z_{Si}	0.206(2)		0.208(1)		0.214(3)		0.204(2)	
z_{Nd}	0.666(2)		0.665(1)		0.665(5)		0.662(1)	
r_{cor}	1.086(7)		1.084(5)		1.090(6)		1.073(3)	
μ_{Mn} (μ_B)			1.90(4)		2.75(4)		2.97(5)	
μ_{Nd} (μ_B)					2.07(3)		2.59(1)	
α (°)					0		110(3)	
R (%)	2.1		2.0		2.8		2.7	

These results suggest that the antiferromagnetic interaction among the manganese spins in the basal plane is dominant and very strong according to the high values of the Néel temperatures observed. Evidence of large antiferromagnetic Mn–Mn interactions is also given by the strongly negative Curie–Weiss temperatures measured in LaMnSi and CeMnSi. Similar results are observed in the isotypic AMnX alkali metal pnictides [14, 15] (*where the manganese sublattice orders as in LaMnSi*) and also in binary compounds such as $FeSn_2$ and $MnSn_2$ [21, 22].

Figure 16 shows the variation in the sign of the intralayer Mn–Mn interaction in the three closely related series of compounds. It appears that in the case of RMnSi a change from ferro to antiferro occurs at about 2.84 Å, while the coupling is always positive for the actually known compounds of the two other structure types in the whole range 2.74–2.97 Å. Moreover, this diagram clearly shows that for the same interatomic Mn–Mn intralayer distance the couplings are inverted between RMnSi and RMn_2Si_2 or $RMnSi_2$ compounds.

Kido *et al.* [13], unfortunately assuming ferromagnetic (001) planes for the RMnSi compounds, have invoked a model based on direct magnetic interaction and related to the Slater–Bethe curve to explain their results. These authors have calculated the radius of the Mn^0 3d orbital by Slater's method [23] and found the ratio $d_{Mn-Mn}/$

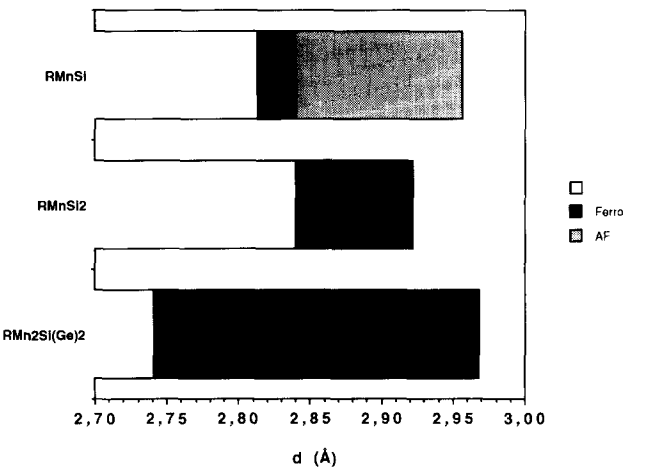

Fig. 16. Evolution of sign of Mn–Mn intralayer interaction *vs.* Mn–Mn intralayer distance in RMnSi (this work), $RMnSi_2$ [9] and $RMn_2Si(Ge)_2$ [8, 10] compounds.

$2r_{3d} = 1.66$ (close to that of Fe metal) yielding the Mn–Mn interaction in the ferromagnetic part of the Slater–Bethe curve. The use of the same 3d orbital radius (about 0.85 Å) also yields ferromagnetic interactions in $RMnSi_2$ and RMn_2Si_2, in agreement with the experimental observations (Fig. 16). In order to explain the antiferromagnetic interaction observed in the RMnSi (R ≡ La–Sm) compounds, this model has to be corrected by assuming a larger spatial extent of the 3d orbital. Furthermore, we would also have to assume that the radius r_{3d} of the Mn atom decreases along the series (from La to Gd or Y), since the Mn layers are ferromagnetic in GdMnSi and YMnSi. Actually, it is difficult to justify such a hypothesis. Nevertheless, the Mn 3d band is different from that found in the RMn_2Si_2 and $RMnSi_2$ compounds, since a significant enhancement of the Mn moment is found in the studied RMnSi series (around 3.3 μ_B in LaMnSi *vs.* 2.1 and 1.9 μ_B in $LaMnSi_2$ and $LaMn_2Si_2$ respectively; see also Tables 4–6 and refs. 8–10).

On the contrary, in the alkali metal manganese pnictides AMnX, where the same antiferromagnetic Mn layers occur, Muller *et al.* [15] have established a correlation between the Mn moment and the interatomic Mn–Mn distances and shown that both increase simultaneously, yielding an Mn moment close to the d^5 configuration in the largest compounds. This correlation is shown in Fig. 17 together with our own data. A fair correlation is found for the isoelectronic AMnX compounds, whereas for similar Mn–Mn distances the moment magnitude is significantly reduced in the silicides. Such effects are in agreement with the difference in ionicity between the pnictides and the silicides on one hand and probably within the silicides on the other.

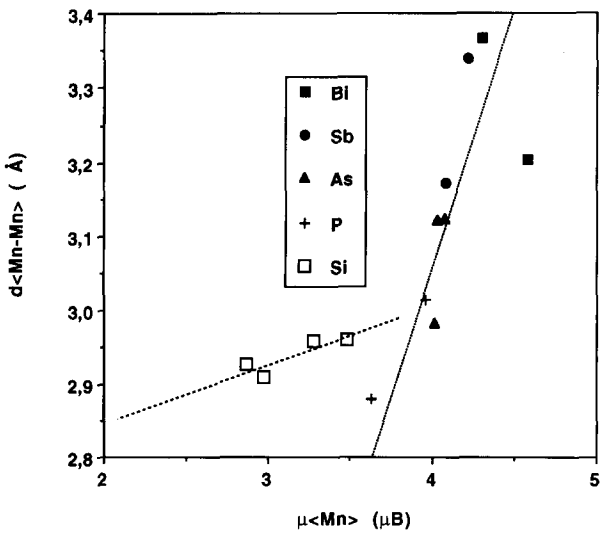

Fig. 17. Mn magnetic moment *vs.* Mn–Mn intralayer distance in equiatomic alkali metal manganese pnictides [14, 15] and RMnSi compounds (this work).

In fact, we observe that the Mn–Si distances are much larger in the RMnSi compounds (about 2.6 Å) than in the $RMnSi_2$ and RMn_2Si_2 ones, where the very small Mn–Si distances (about 2.4 Å) observed suggest covalent-type bonding. Moreover, the decrease in the Mn moments observed in the silicides allows us to interpolate the Mn moment value around the heavy rare earth. For the ferrimagnetic GdMnSi compound and the ferromagnetic YMnSi compound (where an Mn–Si bond length of 2.35 Å [24] is found) the interpolation gives a moment close to 2.2 μ_B, in fair agreement with the saturation moment value observed for GdMnSi at 4.2 K. Following these assumptions, the observed antiferromagnetic Mn layer would be correlated with the high value of the Mn moment. This latter result could be connected to the decrease in the value of the Mn–Si distance in the RMnSi series (from La to Gd) and from RMnSi to RMn_2Si_2 compounds. This latter decrease follows the evolution of the "ionic" to "covalent" character of this bond or at least corresponds to a larger sp–3d overlap. Finally, it is also noteworthy that the Néel temperature of LaMnSi (320 K) is somewhat higher than those of the other members of the series (about 260 K) despite the rare earth contraction, while the Mn moment value decreases from La to Nd (Tables 3–6).

A second model which may be involved is superexchange interaction via the silicon atoms. According to the similarity in bond lengths and bond angles in $RMnSi_2$ and RMn_2Si_2 characterized by ferromagnetic Mn layers, this model would account well for the occurrence of ferromagnetic (001) Mn planes and for the various types of interlayer couplings observed for these compounds.

The distance-dependent oscillatory character of the Ruderman-Kittel-Kasuya-Yoshida (RKKY) interactions may also explain the magnetic property of the RMnSi compounds. This assumption could be corroborated by a difference in the value of the conduction electron concentration between RMn_2Si_2 and RMnSi. Assuming that the electropositive R element donates all its valence electrons to the "MnSi slab", it gives twice as many electrons to this slab in LaMnSi than in $LaMn_2Si_2$ (*i.e.* $3e^-$ in LaMnSi and $1.5e^-$ in $LaMn_2Si_2$ or $2e^-$ in $ThMn_2Si_2$ with the same ferromagnetic sheet [25]). The Mn–Si slab in RMn_2Si_2 is then poorer in electrons than in RMnSi. In order to check this assumption, it would be interesting to examine the magnetic behaviour of the alkaline earth metal ATMnGe compounds (AT ≡ Ca, Sr, Ba) [26] with $2e^-$ in terms of slabs like those in $ThMn_2Si_2$. Band structure calculations on LaMnSi like those performed on $LaMn_2Si_2$ and YMn_2Si_2 [27] might also allow us to get a better understanding of these phenomena.

The second remark concerns the low temperature magnetic structures of the RMnSi (R ≡ La–Nd) series. First we can remark that Pr and Nd order at relatively high temperatures of about 130 and 160 K respectively compared with about 40 K in $PrMnSi_2$, $NdMnSi_2$ and $NdMn_2Si_2$ [9, 10]. It is noteworthy that the Pr sublattice does not order in $PrMn_2Si_2$, at least above 2 K, nor in PrFeSi and PrCoSi(Ge). This point has already been widely discussed in refs. 1, 2, 4 and 10. Moreover, in both compounds the R magnetic moment value is slightly reduced in comparison with the theoretical one and an easy plane prevails. The formal charge attributed to the 3d metal probably has a large effect on the crystal field scheme, since the 3d metal environment of the R site is very asymmetric (Fig. 1). Reduced moment values are also observed in the corresponding $RMnSi_2$ compounds (*e.g.* 2.0 μ_B [9]). Such behaviour is not observed in the RMn_2X_2 parent compounds where the local R symmetry is much higher. The orientation and value of the R moment in such intermetallic compounds have been widely discussed in refs. 1–4, 9 and 10 and the same conclusions probably apply to the RMnSi compounds. Finally it is noteworthy that the R intralayer coupling is the same in the three series, *i.e.* ferromagnetic.

The most remarkable point is the rather high ordering temperature observed in those compounds characterized by a rare earth site which experiences no molecular field according to the tetragonal symmetry and the occurrence of antiferromagnetic Mn planes. The strength of the interactions is quite different from that observed in related compounds. In other CeFeSi-type compounds the ordering temperatures are much lower (NdCoGe, $T_N = 8$ K [2]; NdFeSi, $T_C = 25$ K [1]; NdRuSi, $T_N = 72$ K [3]) than in RMnSi ones. In $TbFeSi_2$ compounds such as $PrMnSi_2$ ($T_t = 35$ K) and $NdMnSi_2$ ($T_t = 40$ K) [9] characterized by ferromagnetic Mn layers, the rare earth site experiences a molecular field and the ordering temperatures are still lower than in RMnSi. Finally, in $ThCr_2Si_2$-type compounds the ferromagnetic Mn layers are ferromagnetically or antiferromagnetically coupled, giving rise to a substantial or no molecular field on the rare earth site respectively. In both cases the rare earth orders below the ordering temperature of the RMnSi compounds. In the ferromagnetic $NdMn_2Si_2$ compound, for example, $T_C = 33$ K. In the case of $CeMnSi_2$ the situation is much more surprising, since an ordering temperature of about 180 K is observed. It should be noted that Ce is trivalent in $CeMnSi_2$ [9] (with no ordering scheme above 2 K), whereas a recent study has shown that it has an intermediate valence state in $CeMn_2Si_2$ [28].

The high ordering temperature of the rare earth element is thus correlated with the occurrence of antiferromagnetic Mn layers. Such correlations are probably due to a particular electronic structure (yielding high Mn moment values and antiferromagnetic coupling) leading to unusual strengths of the interactions involving the rare earth moments.

The magnetic ordering of the rare earth and transition metal sublattices involves three main types of exchange interactions: T–T, R–T and R–R. In rare-earth-poor systems such as permanent magnet compounds the R–R interactions are generally considered to be negligible in comparison with the R–T and T–T interactions. Within the present rare-earth-rich silicides it will be rather difficult to separate the contributions of the R–R and R–T interactions from the observed R sublattice ordering.

The magnetic properties of ternary rare earth compounds are still not well explained. The magnetic interactions involving rare earth moments are generally described within the RKKY model [29]. Owing to the localized character of the 4f shells, one assumes indirect exchanges via a distance-dependent oscillatory polarization of the conduction electrons which interacts with any magnetic moment in the crystal. Campbell [30] has proposed a mechanism involving intra-atomic 4f–5d exchange combined with direct d–d interatomic exchange. On strictly empirical grounds this author has shown that at short range in any case the hypothesis of positive f–d exchange and direct d–d interactions is more justified than the RKKY formulation. Another model has been developed by Cooper *et al.* [31] on the basis of the partially delocalized behaviour of the 4f electrons in the lighter rare earths. This so-called "orbitally driven magnetism" accounts well for the anisotropic magnetism observed in the studied compounds. For the lighter rare earths (Ce, Pr, Nd), the degree of delocalization depends on the detailed chemical environment and decreases with the atomic number.

Attempts to explain the observed magnetic behaviour on the basis of these previous considerations may be made. First, the magnetic R ordering within the "W slab" may be related to the Campbell mechanism. In this slab the R–R contacts are rather short and allow direct 5d–5d exchange. The model accounts well for the ferromagnetic interactions observed in PrMnSi and NdMnSi. A similar slab is found in ferromagnetic NdGe and PrGe [32] with much lower Curie temperatures. The coupling between two adjacent "W slabs" through the Mn layer may lead either to R–Mn interactions or to indirect exchange through the $BaAl_4$ slab mediated by conduction electrons. Since the rare earth site is surrounded by four equidistant manganese atoms of which half have their spin up and half have their spin down, isotropic couplings cannot account for any exchange. Assuming partially delocalized 4f electrons, an "orbitally driven magnetism" may be invoked to explain the R–Mn couplings. Assuming that the rare earth

moment is along the [010] direction (see before), the disk-like 4f cloud should be parallel to the (010) plane and then overlap with the 3d shells of the Mn atoms lying in the same plane (the (P) plane previously defined in Section 4.3.2), *i.e.* with those which have the same moment direction. The other possible mechanism is R–R indirect exchange via the conduction electrons and the oscillatory character of the polarization. This mechanism, which is responsible for the long-range ordering in the isotypic RTSi compounds where T is non-magnetic, gives rise to much lower ordering temperatures. When this model is invoked here, one has to assume a mechanism reinforcing the corresponding interactions, such as a modification of the RKKY parameters or a particular scattering of the conduction electrons through the antiferromagnetic Mn layer, which could enhance the amplitude of the oscillatory wave.

Below about 80 K a strong magnetostriction effect occurs as observed in the RFeSi compounds. This effect is clearly observed in PrMnSi and NdMnSi. The chemical cells of PrMnSi and NdMnSi are distorted (from tetragonal to orthorhombic symmetry), yielding two sets of interatomic R–Mn distances (see above). The R–Mn coupling is ferromagnetic (*i.e. the normal behaviour between a 3d transition metal and a light rare earth*) between nearest neighbours and gives rise to spin reorientation phenomena of the Mn sublattice, the relative R and Mn sublattice orderings remaining unchanged. The splitting of the R–Mn distances allows for additional isotropic exchange couplings. It is noteworthy that the low temperature magnetic structures of PrMnSi and NdMnSi are slightly different. In the case of NdMnSi, the reorientation of the Mn sublattice is only partial and gives evidence of the strong anisotropy of the easy magnetization axis of the Nd sublattice and the Mn sublattice which probably causes the observed behaviour. It is noteworthy that the same behaviour occurs in $PrMnSi_2$, $NdMnSi_2$ and $NdMn_2Si_2$, in which compounds the strength of the interactions is of similar magnitude.

6. Conclusions

The analysis of the magnetic ordering of RMnSi (R ≡ La, Ce, Pr, Nd) compounds provides interesting information about the magnetic anisotropy and exchange interactions in this series.

At high temperature an antiferromagnetic ordering of the Mn sublattice was found in all the compounds investigated, with an Mn moment of 2.8–3.3 μ_B perpendicular to the stacking axis of the structure. Comparison with the parent RMn_2X_2, $ThCr_2Si_2$-type compounds shows that the sign of the Mn–Mn intralayer exchange parameter seems to be sensitive to the Mn–Mn intralayer separation and that the Mn–Si distance correlates with the value of the Mn moment. In order to check this point, further investigations on corresponding germanides and alkaline earth metal manganese compounds (ATMnSi(Ge) with AT ≡ Ca–Ba) are in progress. It would also be interesting to check the magnetic ordering in YMnSi and to examine the evolution of the Mn–Mn intralayer couplings in solid solution $La_{1-x}Y_xMnSi$.

The understanding of the magnetic ordering of the R sublattice in RMnSi compounds probably requires more sophisticated models than the exchange interactions described by the RKKY mechanism. Nevertheless, comparison of the RTSi, $RTSi_2$ and RT_2Si_2 series permits us to point out that at low temperature the exchange interactions between R and Mn atoms play a significant role in the magnetic ordering. Furthermore, the magnetic configurations not only depend on the R ion but also vary with the transition metal element T. At low temperature the direction of the magnetic moment is not fixed for a given T, but the easy direction is determined by the crystalline electric field acting on the R ions. The orientation of the magnetic moment is connected with the sign of the B_2^0 CEF coefficient, which in turn is determined by the Stevens second-order parameters α_j and by A_2^0. Since the Stevens factor α_j depends only on the nature of R, the crucial factor is A_2^0, which is determined by the electrostatic potential due to the environment.

The magnitudes of the R magnetic moments in RMnSi are somewhat smaller than the corresponding free-ion values, in contrast with the RT_2X_2 compounds. Most likely this must be attributed to CEF effects. Finally, in order to understand more about the magnetic configurations on the R and T sublattices and the high ordering temperature observed on the Ce sublattice of CeMnSi, further investigations using Mn and Nd nuclear magnetic resonance spectroscopy and specific heat measurements are in progress.

Acknowledgments

Neutron diffraction data were recorded at the Institut Laue Langevin (ILL). We are grateful to J.L. Soubeyroux, responsible for the spectrometer used, for his help during the measurements.

References

1 R. Welter, G. Venturini and B. Malaman, *J. Alloys Comp., 189* (1992) 49.
2 R. Welter, G. Venturini, B. Malaman and E. Ressouche, *J. Alloys Comp., 201* (1993) 191.

3 R. Welter, G. Venturini, B. Malaman and E. Ressouche, *J. Alloys Comp., 202* (1993) 165.
4 R. Welter, G. Venturini, B. Malaman and E. Ressouche, *J. Alloys Comp.,* to be published.
5 O.I. Bodak, E.I. Gladyshevskii and P.I. Kripyakevich, *J. Struct. Chem., 11* (1970) 1861.
6 Z. Ban and M. Sikirika, *Acta Crystallogr., 18* (1965) 594.
7 V.I. Yarovets and Yu.K. Gorenlenko, *Vest. L'vovsk. Univ., Ser. Khim., 23* (1981) 20.
8 A. Szytula and J. Leciejewicz, Magnetic properties of ternary intermetallic compounds of the RT_2X_2 type, in K.A. Gschneidner Jr. and L. Eyring (eds.), *Handbook on the Physics and Chemistry of Rare Earths,* Vol. 12, Elsevier, Amsterdam, 1989, Chap. 83, p. 133.
9 B. Malaman, G. Venturini, L. Pontonnier and D. Fruchart, *J. Magn. Magn. Mater., 86* (1990) 349.
10 R. Welter, G. Venturini, D. Fruchart and B. Malaman, *J. Alloys Comp., 191* (1993) 263.
11 V.I. Yarovets and Yu.K. Gorenlenko, *Vest. L'vovsk. Univ., Ser. Khim., 23* (1981) 20.
12 S.A. Nikitin, T.I. Ivanova, O.V. Nekrasova, R.S. Torchinova, Yu.F. Popov, O.N. Koryasova and Ye.A. Klyucnikova, *Fiz. Met. Metall., 64*(6) (1987) 1071.
13 H. Kido, T. Hoshikawa, M. Tagami, M. Shimada and M. Koizumi, *J. Ceram. Assoc. Jpn., 94*(1) (1986) 232.
14 W. Bronger, P. Muller, R. Hoppner and H.U. Schuster, *Z. Anorg. Allg. Chem., 539* (1986) 175.
15 R. Muller, M. Kuckel, H.U. Schuster, P. Muller and W. Bronger, *J. Alloys Comp., 176* (1991) 167.
16 E. Parthé and B. Chabot, in K.A. Gschneidner Jr and L. Eyring (eds.), *Handbook on the Physics and Chemistry of Rare Earths,* Vol. 6, North-Holland, Amsterdam, 1984, p. 113.
17 C.G. Shull and Y. Yamada, *J. Phys. Soc. Jpn., 22* (1962) 1210.
18 C. Stassis, H.W. Deckman, B.N. Harmon, J.P. Desclaux and A.J. Freeman, *Phys. Rev. B, 15* (1977) 369.
19 P. Wolfers, *J. Appl. Crystallogr., 23* (1990) 554.
20 C. Godart, personal communication, 1993.
21 G. Venturini, B. Malaman, G. Le Caër and D. Fruchart, *Phys. Rev. B, 35*(13) (1987) 7038.
22 G. Le Caër, B. Malaman, G. Venturini and I.E. Kim, *Phys. Rev. B, 26*(9) (1982) 2010.
23 J.C. Slater, *Phys. Rev., 36* (1930) 57.
24 H. Kido, T. Hoshikawa, M. Shimada and M. Koizumi, *Phys. Status Solidi A, 88* (1985) K39.
25 Z. Ban, L. Omejec, A. Szytula and Z. Tomkowicz, *Phys. Status Solidi A, 27* (1975) 333.
26 W. Dörrscheidt and H. Schäfer, *Z. Natur. Anorg. Chem. B, 31* (1976) 1050.
27 S. Ishida, S. Asano and J. Ishida, *J. Phys. Soc. Jpn., 55*(3) (1986) 936.
28 G. Liang, I. Perez, D. Dimarzio, M. Craft, D.C. Johnston, N. Anbalagon and T. Mihalisin, *Phys. Rev. B, 37* (1988) 5970.
29 P.G. de Gennes, *J. Phys. Radium, 23* (1962) 510.
30 I.A. Campbell, *J. Phys. F: Met. Phys., 2* (1972) L47.
31 B.R. Cooper, J.M. Wills, N. Kioussis and Q.G. Sheng, *J. Phys. (Paris), 49* (1988) 463.
32 P. Schobinger-Papamantellos and K.H.J. Buschow, *J. Less-Common Met., 111* (1985) 125.